Journal of Power Sources 196 (2011) 6042–6047

Contents lists available at ScienceDirect

Journal of Power Sources

journal homepage: www.elsevier.com/locate/jpowsour

An H_3PO_4-doped polybenzimidazole/$Sn_{0.95}Al_{0.05}P_2O_7$ composite membrane for high-temperature proton exchange membrane fuel cells

Y.C. Jin [a], M. Nishida [b], W. Kanematsu [b], T. Hibino [a,*]

[a] Graduate School of Environmental Studies, Nagoya University, Chikusa-ku, Nagoya 464-8601, Japan
[b] Research Institute Instrumentation Frontier, National Institute of Advanced Industrial Science and Technology, Moriyama-ku, Nagoya 463-8560, Japan

ARTICLE INFO

Article history:
Received 8 March 2011
Received in revised form 30 March 2011
Accepted 30 March 2011
Available online 6 April 2011

Keywords:
Composite membrane
Proton conductor
Tin diphosphate
Polybenzimidazole
High-temperature proton exchange membrane fuel cell

ABSTRACT

A polybenzimidazole (PBI)/$Sn_{0.95}Al_{0.05}P_2O_7$ (SAPO) composite membrane was synthesized by an *in situ* reaction of SnO_2 and $Al(OH)_3$-mixed powders with an H_3PO_4 solution in a PBI membrane. The formation of a single phase of SAPO in the PBI membrane was completed at a temperature of 250 °C. Thermogravimetric analysis showed that the PBI membrane was not subject to a serious damage by the presence of SAPO until 500 °C. Scanning electron microscopy revealed that SAPO particles with a diameter of approximately 300 nm were homogeneously dispersed and separated from each other in the PBI matrix. Proton magic angle spinning nuclear magnetic resonance spectra confirmed the presence of new protons originating from the SAPO particles in the composite membrane. As a consequence of the interaction of protons in the SAPO with those in the free H_3PO_4, the H_3PO_4-doped PBI/SAPO composite membrane exhibited conductivities several times higher than those of an H_3PO_4-doped PBI membrane at room temperature to 300 °C, which could contribute to the improved performance of H_2/O_2 fuel cells.

1. Introduction

In recent years, proton exchange membrane fuel cells (PEMFCs) capable of operating at temperatures above 100 °C have received great attention due to their advantages over low-temperature PEMFCs based on perfluorosulphonic acid polymer electrolytes (e.g., Nafion). These advantages include faster electrode reaction kinetics, better CO tolerance, and simpler heat and water management [1–4]. Consequently, the development of high-temperature PEMFCs has been aggressively pursued for their early commercialization. Among the candidate electrolyte materials developed to date, H_3PO_4-doped polybenzimidazole (PBI) is regarded as one of the most promising alternative electrolytes [5–7]. The PBI membrane functions as a proton-conducting electrolyte by doping with H_3PO_4, wherein the proton conductivity is dependent on the H_3PO_4 content in the PBI membrane. Kawahara et al. reported that at a low acid doping level of 1.9 (mole number of H_3PO_4 per repeat unit of polymer), the proton conductivity was as low as 10^{-5} S cm^{-1} at a temperature of 160 °C because all doped H_3PO_4 were strongly restricted in the polymer matrix by hydrogen bonds [8]. In contrast, at high acid doping levels of 4–6, the proton conductivity reached 4–7 × 10^{-2} S cm^{-1} under the same conditions. These results demonstrated that the presence of free H_3PO_4 is a prerequisite for high proton conductivity. The good mechanical properties of PBI membranes also make them attractive for fuel cell applications, but their mechanical strength is reduced with an increase in the acid doping level due to the plastifying effect of the excessive free H_3PO_4 [9]. There is therefore a trade-off between proton conductivity and mechanical strength.

One promising approach for avoiding the above problem is to prepare composites of PBI with various proton-conducting solid acids. Metal phosphates [10], heteropoly acids [11–13], partial Cs+-substituted heteropoly acids [14,15], and zirconium tricaboxybutylphosphonate [16,17] have been examined as solid acids. For instance, He et al. found that when $Zr(HPO_4)_2{\cdot}nH_2O$ was incorporated into a PBI membrane, the proton conductivity at a relatively low H_3PO_4 doping level was increased by approximately 50% [10]. Similarly, Oh et al. reported that the proton conductivity of a PBI/$CsHSO_4$–$H_3PW_{12}O_{40}$ or $H_4SiW_{12}O_{40}$ composite membrane with a relatively low H_3PO_4 doping level was comparable to that of a pure PBI membrane with a high H_3PO_4 doping level [14]. A further increase in the proton conductivity would enhance the position of PBI-based composite membranes as preferred high-temperature proton-exchange membranes.

More recently, $Sn_{0.95}Al_{0.05}P_2O_7$ (SAPO) has been reported to show high proton conductivities (~0.1 S cm^{-1}) in a high-temperature range, i.e., 100–300 °C [18,19]. Another unique feature of this material is that its conductivity increases monotonically with increasing temperature, rather than exhibiting superprotonic behavior, which is associated with a sharp increase in the conductivity of some orders of magnitude due to a structural transition from a low- to a high-temperature phase [20].

* Corresponding author. Tel.: +81 52 789 4888; fax: +81 52 789 4894.
E-mail address: hibino@urban.env.nagoya-u.ac.jp (T. Hibino).

0378-7753/$ – see front matter © 2011 Elsevier B.V. All rights reserved.
doi:10.1016/j.jpowsour.2011.03.094

These characteristics motivate the development of a new composite membrane comprising PBI and SAPO. In this study, we investigated an H_3PO_4-doped PBI/SAPO composite membrane for high-temperature PEMFC applications. An *in situ* synthesis of SAPO in the PBI membrane was carried out by the addition of SnO_2 and $Al(OH)_3$ powders to the PBI membrane, followed by the reaction of these powders with a doped H_3PO_4 solution. The composite membrane obtained was characterized by various means, including X-ray diffraction (XRD), thermogravimetric and differential thermal analysis (TG–DTA), scanning electron microscopy (SEM), magic angle spinning nuclear magnetic resonance (MAS NMR), and electrochemical impedance spectroscopy (EIS) techniques. Finally, the performance and short-term stability of a H_2/O_2 fuel cell with this composite membrane was evaluated in the temperature range from 100 to 200 °C.

2. Experimental

2.1. Preparation of the composite membrane

A PBI/SAPO composite membrane was prepared as follows. Reagent-grade SnO_2 (Wako Chemicals) and $Al(OH)_3$ (Wako Chemicals) were used as source materials for synthesis of SAPO. SnO_2 and $Al(OH)_3$ (95/5 molar ratio) powders were mixed in tetrahydrofuran (THF, Wako Chemicals) using a Fritsch Pulverisette 5 planetary ball mill at 150 rpm for 6 h and then dried at 50 °C for 1 h to evaporate the THF solvent. PBI (10 wt% in N, N-dimethyl acetamide (DMAc)) was purchased from AZ Electronic Materials. The SnO_2 and $Al(OH)_3$-mixed powder (0.382 g) was added to the PBI solution (5.0 g). After grinding using a ball mill at 150 rpm for 16 h, the slurry was cast onto a glass substrate using a doctor blade, and then dried first at 90 °C in air for 1 h and finally under vacuum at 120 °C for 4 h. Subsequently, the membrane (PBI/SnO_2–$Al(OH)_3$) was peeled off from the surface of the glass substrate. For comparison, a pure PBI membrane was also made by casting the PBI solution onto the glass substrate, followed by the same treatment described above. The thickness of both the PBI/SnO_2–$Al(OH)_3$ composite and pure PBI membranes was controlled by changing the gap of the opening blade. The PBI/SnO_2–$Al(OH)_3$ composite membrane was immersed in an 85% H_3PO_4 solution at 60 °C overnight. The surface of the H_3PO_4-doped PBI/SnO_2–$Al(OH)_3$ composite membrane was carefully wiped to remove the residual H_3PO_4 present on the surface. The composite membrane was then calcined in a feed mixture of 10% H_2 and Ar in the temperature range from 150 to 250 °C for 4 h. Finally, the PBI/SAPO composite membrane obtained was cut into test samples of an appropriate size.

2.2. Estimation of the H_3PO_4 doping level

An H_3PO_4 doping process was conducted by immersing the PBI/SAPO composite and PBI membranes into the 85% H_3PO_4 solution at a temperature of 65 °C. For the PBI membrane, the H_3PO_4 doping level was estimated according to the following equation.

$$H_3PO_4 \quad \text{doping level}\,(\%) = \frac{W - W_p}{W_p} \times 100 \tag{1}$$

where W and W_p are the membrane weights after and before doping with H_3PO_4, respectively. For the PBI/SAPO composite membrane, unreacted H_3PO_4 existed in the as synthesized composite membrane. To obtain information on the weight of the H_3PO_4-free PBI/SAPO composite membrane, the composite membrane was washed with ethanol, followed by drying at a temperature of 120 °C. Accordingly, W and W_p represented in Eq. (1) are the membrane weights after doping with H_3PO_4 and after washing with ethanol, respectively.

2.3. Materials characterization

The membrane samples were characterized by XRD, SEM with an energy dispersive X-ray (EDX) detector, TG–DTA, ^1H and ^{31}P MAS NMR, and EIS. The XRD patterns were recorded using a Rigaku Miniflex II diffractometer with Cu Kα radiation (λ = 1.5432 Å) as the X-ray source. The diffractometer was operated at 45 kV and 20 mA. The SEM/EDX images were obtained using a Hitachi S-4800 at an accelerating voltage of 5 kV with a beam current of 0.2 nA. The TG–DTA curves were observed using a Shimadzu DTG-60 from room temperature to 550 °C in air at a heating rate of 10 °C min^{-1}. The NMR spectra were measured using a Varian Unity Inova 300 NMR spectrometer employing a pulse length of 5 μs, a decay time between pulses of 10 s and a sample spinning rate of 9 kHz. The AC conductivity measurements were performed in unhumidified air using a Solartron SI 1260 impedance analyzer with two Au plates as the electrodes and an AC amplitude of 20 mV at frequencies ranging from 100 kHz to 0.1 Hz.

2.4. Fuel cell tests

An H_2/O_2 fuel cell was fabricated using a membrane sample as an electrolyte. A commercially available catalyzed gas diffusion layer (BASF, Pt loading: 4 mg cm^{-2}) was used for both the anode and cathode (area: 0.5 cm^2). The electrolyte membrane was sandwiched between the two electrodes and hot-pressed at 150 °C and 2 MPa for 10 min. Two gas chambers were set up by placing the cell assembly between two alumina tubes, with each chamber sealed using an inorganic adhesive. Unhumidified H_2 (30 mL min^{-1}) and O_2 (60 mL min^{-1}) were supplied to the anode and cathode, respectively, over the temperature range from 100 to 200 °C. The current–voltage curves were measured using a Hokuto Denko HA-501 galvanostat. The ohmic and electrode-reaction resistances were separated by the above-mentioned EIS technique.

3. Results and discussion

3.1. Preparation of the PBI/SAPO composite membrane

Firstly we attempted to synthesize a PBI/SAPO composite membrane directly from a SAPO and PBI-mixed slurry. This slurry was obtained by grinding the SAPO powder with the PBI solution in the ball mill. After casting the slurry on the glass substrate, the mold was dried at 120 °C under vacuum for 4 h. It can be seen in Fig. 1(a) that the membrane obtained using this procedure broke into pieces and thus the function of PBI as a binder was lost. This result may be due to a neutralization reaction between PBI and SAPO. It is well known that PBI membranes are difficult to cast directly from PBI and H_3PO_4-mixed solutions because of the formation of a hydrogen bond between the NH group in the amidazole ring of PBI and a proton of the H_3PO_4 molecule [21,22]. A similar phenomenon is thought to have occurred in the present case. (For this reason, we previously fabricated a PBI/SAPO composite membrane by using polytetrafluoroethylene (PTFE) as a binder [23].) In the present study, however, a PBI/SnO_2–$Al(OH)_3$ composite membrane could be easily formed with a high degree of mechanical strength (Fig. 1(b)). Furthermore, this membrane was found to be stable, even when reacted with H_3PO_4 at a relatively high temperature of 250 °C (Fig. 1(c)).

The growth of SAPO particles in the PBI membrane was evaluated by examining the XRD patterns of membranes prepared at reaction temperatures varying from 150 to 250 °C (Fig. 2). The as-immersed membrane sample shows only diffraction peaks assigned to the SnO_2 tetragonal structure. (No $Al(OH)_3$ peaks were observed, probably due to its minimal content level.) The SnO_2

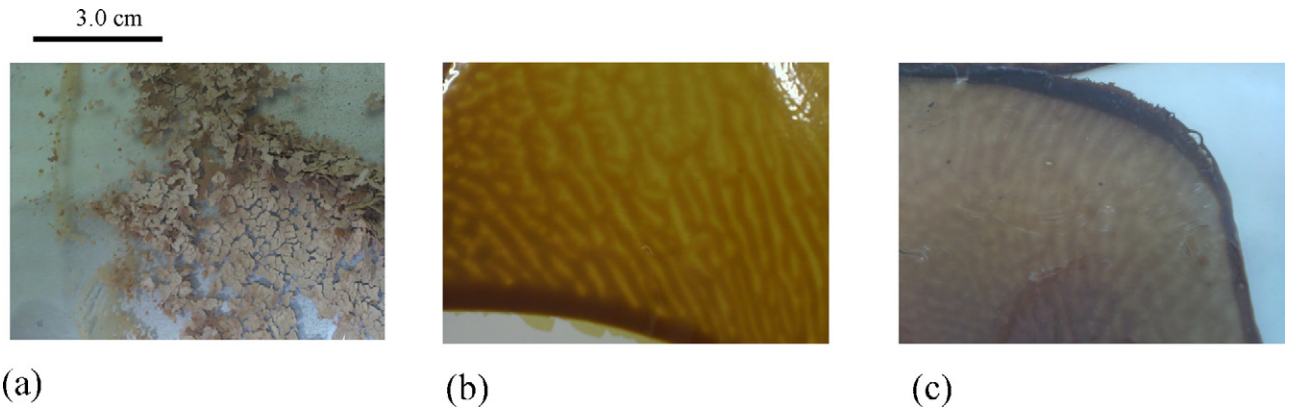

Fig. 1. Photographs of (a) the membrane prepared from a SAPO and PBI-mixed slurry, (b) the membrane prepared from an SnO_2, $Al(OH)_3$, and PBI-mixed slurry, and (c) the membrane prepared by the reaction of the membrane in (b) with H_3PO_4 at 250 °C.

peaks remained until the temperature reached 200 °C, at which point diffraction peaks attributed to the SnP_2O_7 cubic structure appeared. These results suggest that the following reaction proceeded in the composite membrane.

$$(1-x)SnO_2 + xAl(OH)_3 + 2H_3PO_4 \rightarrow Sn_{1-x}Al_xP_2O_7 + yH_2O \quad (2)$$

A single crystal phase of SAPO could be obtained when the temperature was raised to 250 °C. At that time, the SAPO content accounted for 60 wt% of the total composite membrane. The mean particle size of SAPO, estimated using the Scherrer formula, was found to be 18 nm, which is considerably smaller than the approximately 300 nm size estimated for the SAPO agglomerates from the SEM measurement (vida supra).

3.2. Characterization of the PBI/SAPO composite membrane

Several techniques were employed to determine the important characteristics of the PBI/SAPO composite membrane. TG–DTA curves of PBI, SAPO, and PBI/SAPO samples are shown in Fig. 3. The PBI membrane sample showed a weight loss of about 5% and a small endothermic peak between 50 and 130 °C that is due to the desorption of adsorbed or absorbed water from PBI. Additionally, a remarkable endothermic peak was observed along with a weight loss of about 5% above 450 °C, which indicates the thermal decomposition of PBI. The SAPO powder sample showed no weight loss until 150 °C. Beyond this temperature, the weight was gradually reduced by about 5%. As reported previously [24], this weight loss is attributable to the desorption of protons incorporated into the SAPO crystals. The PBI/SAPO composite membrane showed two distinct endothermic peaks that were accompanied by respective small weight losses: one between 50 and 150 °C and another between 150 and 250 °C. Although the former can be attributed to the desorption of adsorbed or absorbed water, the latter can be considered to be the result of the dehydration reaction of residual H_3PO_4 in the composite membrane [25]. The TG–DTA curves above 250 °C were similar to those observed for the SAPO powder sample, which suggests that the PBI membrane is not seriously damaged by the presence of SAPO until at least 500 °C.

Morphological analysis of the PBI/SAPO composite membrane was conducted using SEM/EDX. Cross-sectional SEM/EDX images of the whole composite membrane are displayed in Fig. 4. The SEM image reveals agglomeration of the SAPO particles with several aggregates reaching sizes of several tens of micrometers, whereas the EDX images clearly show a nearly homogeneous dispersion of P and Sn (green in the P and Sn mapping) throughout the cross-section of the composite membrane. Notably, the composite membrane was considerably dense and pinhole and crack free. High magnification SEM images presented in Fig. 5 provide detailed information on the microstructure of the SAPO particles in the composite membrane. There were numerous SAPO particles with a diameter of approximately 300 nm (white in the SEM image), which seemed to be agglomerates of SAPO crystals. Moreover, the SAPO particles were not closely packed with each other, and their connection was partially broken by PBI (grey in the SEM image).

The doping of the PBI/SAPO composite membrane with H_3PO_4 was carried out at a temperature of 60 °C, and the H_3PO_4 doping level was estimated according to Eq. (1). Fig. 6 shows the H_3PO_4 doping level as a function of the doping time for the pure PBI and PBI/SAPO composite membranes. The PBI/SAPO composite membrane reached the saturation level after approximately

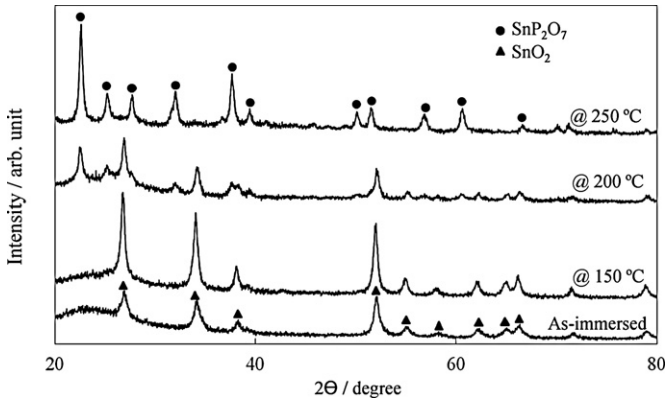

Fig. 2. XRD patterns of the membrane after reaction with H_3PO_4 at various temperatures.

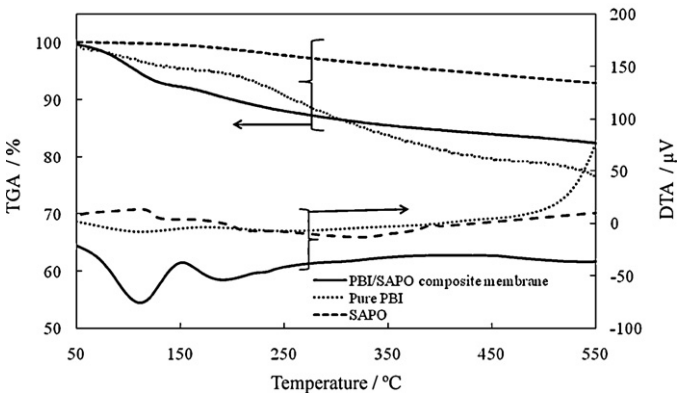

Fig. 3. TG–DTA curves of PBI, SAPO, and PBI/SAPO composite membrane samples.

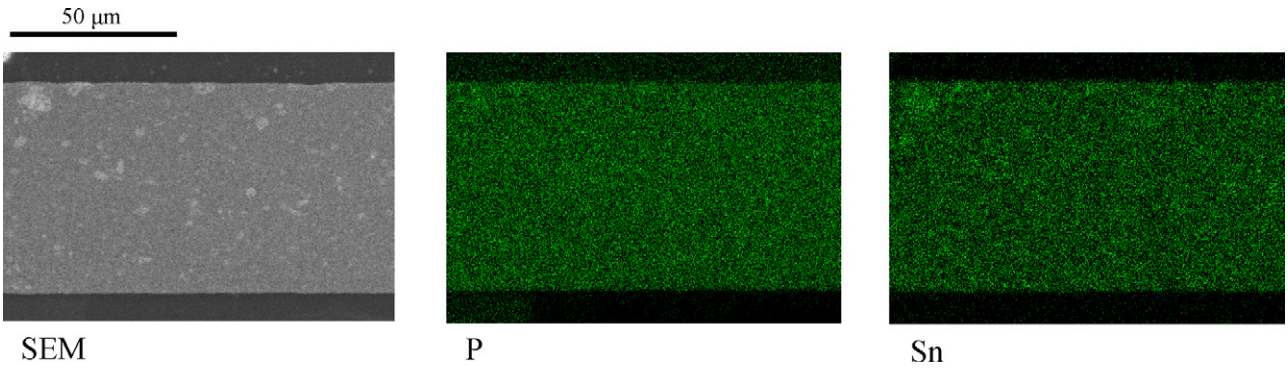

Fig. 4. SEM micrographs and P and Sn element mappings of the cross-section of the PBI/SAPO composite membrane.

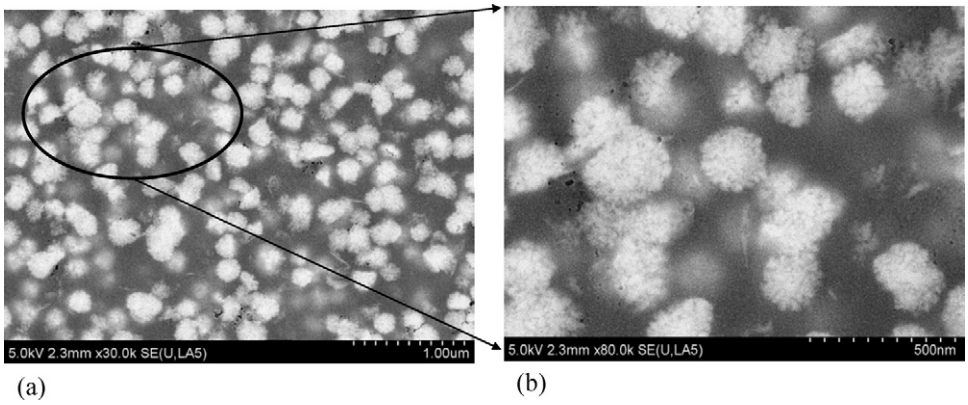

Fig. 5. High-magnification SEM micrographs of SAPO particles in the PBI/SAPO composite membrane.

15 h, whereas the PBI membrane was filled up with H_3PO_4 after only about 4 h. The maximum H_3PO_4 doping level observed for the PBI/SAPO composite membrane was 114 wt%. Considering the PBI content of 40 wt% in the composite membrane, the net H_3PO_4 doping level is calculated to be 285 wt%, which is still smaller than the maximum H_3PO_4 doping level of 375 wt% for the PBI membrane. It is likely that the presence of the SAPO particles suppresses the permeation of H_3PO_4 into the PBI membrane.

The phosphorous and proton environments in the H_3PO_4-doped PBI/SAPO composite membrane were characterized by solid-state NMR spectroscopy. ^{31}P NMR spectra for the H_3PO_4-doped composite and pure PBI membranes are shown in Fig. 7(a). Both of the samples displayed one sharp resonance peak centered near 0 ppm. The peak intensity of the H_3PO_4-doped PBI/SAPO composite membrane was lower than that of the H_3PO_4-doped PBI membrane, which reflects the difference in H_3PO_4 doping levels between the two samples (vida infra). On the other hand, as shown in Fig. 7(b), the ^1H NMR spectrum of the H_3PO_4-doped PBI/SAPO composite membrane revealed two distinct resonance peaks centered at 9.2 and 8.3 ppm, while the H_3PO_4-doped PBI membrane showed only one peak centered at 9.1 ppm. The resonance peak at 8.3 ppm observed for the H_3PO_4-doped PBI/SAPO composite membrane originates from protons incorporated into the SAPO powder. Indeed, in the NMR spectrum of the SAPO powder, the main resonance peak was observed at nearly the same chemical shift.

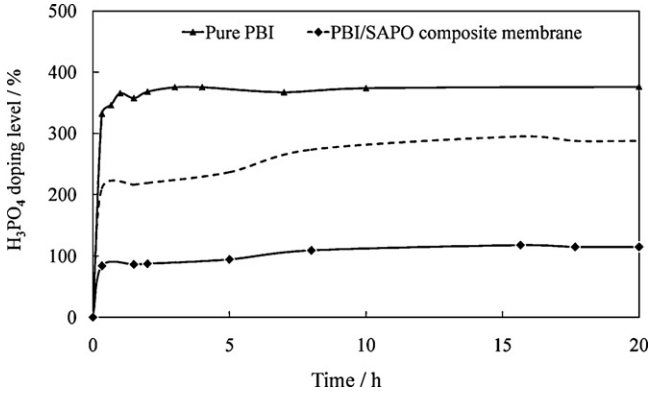

Fig. 6. H_3PO_4 doping levels for the PBI/SAPO composite and PBI membranes as a function of immersion time in an 85% H_3PO_4 solution at 60 °C. The dotted line represents the net H_3PO_4 doping level estimated for the 40 wt% PBI membrane.

The proton conductivity of the H_3PO_4-doped PBI/SAPO composite membrane was measured and compared with the proton conductivity of the H_3PO_4-doped PBI membrane. Fig. 8 shows that the H_3PO_4-doped PBI/SAPO composite membrane exhibited higher conductivities than those of the H_3PO_4-doped PBI membrane. For instance, the proton conductivity of the former was 0.034 S cm^{-1} at 150 °C and 0.032 S cm^{-1} at 200 °C as compared to 0.011 S cm^{-1} at 150 °C and 0.015 S cm^{-1} at 200 °C for the latter. It should be noted that the proton conductivities of both the membranes above 200 °C were not reproducible during thermal cycling, due to the dehydration reaction of H_3PO_4. The ^1H MAS NMR spectra revealed no change in the chemical shift of the H_3PO_4- and SAPO-related peaks for the composite membrane, which suggests no formation of new proton species with a fast mobility at the interface of SAPO and PBI. One possible explanation for these observations is the interaction of protons in the SAPO particles with those in the H_3PO_4 molecules. As described earlier, the relative density of the SAPO particles in the composite membrane was too low to provide networks of proton pathways predicted by the Percolation theory [26]. There is a large electrical resistance between the SAPO particles. Such an electri-

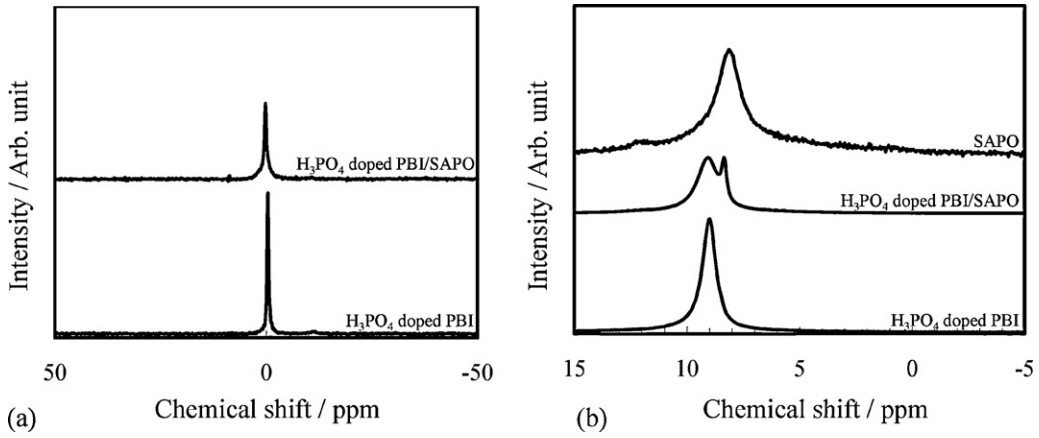

Fig. 7. (a) ^{31}P MAS NMR spectra and (b) ^{1}H NMR spectra of the H_3PO_4-doped PBI/SAPO composite membrane and the H_3PO_4-doped PBI membrane.

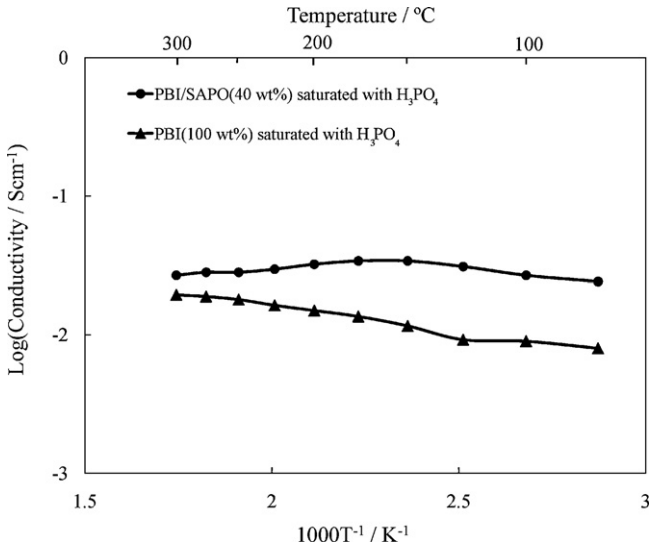

Fig. 8. Proton conductivities of the H_3PO_4-doped PBI/SAPO composite membrane and the H_3PO_4-doped PBI membrane in air.

cal resistance would be significantly reduced by the presence of free H_3PO_4 molecules around the SAPO particles, because the free H_3PO_4 molecules form a proton pathway from one SAPO particle to another. This mechanism is supported by the fact that the proton conductivity of a non-doped PBI/SAPO composite membrane was as low as 0.002 S cm^{-1} at 200 °C.

3.3. Cell performance and lifetime

Next, the performance of the H_3PO_4-doped PBI/SAPO composite membrane was evaluated in an H_2/O_2 fuel cell. The cell performance was tested for a 45-μm-thick H_3PO_4-doped PBI/SAPO composite membrane over the temperature range from 100 to 200 °C under unhumidified conditions. The current–voltage curves of the fuel cell are shown in Fig. 9(a). At all temperatures tested, an open circuit potential of approximately 1 V was obtained, which indicates that the crossover of H_2 or O_2 through the composite membrane is negligible. In addition, the current–voltage slopes decreased as the operating temperature increased from 100 to 200 °C. Consequently, the peak power density reached 234.6 mW cm^{-2} at 100 °C, 342.2 mW cm^{-2} at 150 °C and 439.6 mW cm^{-2} at 200 °C. For comparison, fuel cell tests for the H_3PO_4-doped PBI membrane with a thickness of 45 μm were also conducted. As show in Fig. 9(b), the peak power densities obtained were 215.6, 285.6, and 369.4 mW cm^{-2} at 100, 150, and 200 °C, respectively, which are lower than those for the H_3PO_4-doped PBI/SAPO composite membrane. From the impedance spectra of these fuel cells, it was found that the difference in cell performance observed is mainly due to the difference in ohmic resistance between them: 0.19 Ω cm^2 at 200 °C for the H_3PO_4-doped PBI/SAPO composite membrane and 0.30 Ω cm^2 at 200 °C for the H_3PO_4-doped PBI membrane. It is also worth noting that the characteristics of the composite membrane were achieved at a relatively low H_3PO_4 doping level.

Finally, the cell voltage of the fuel cells with the PBI/SAPO composite and PBI membranes was monitored during cell discharge at 150 °C. The cell voltages of the two gradually decreased with a slope

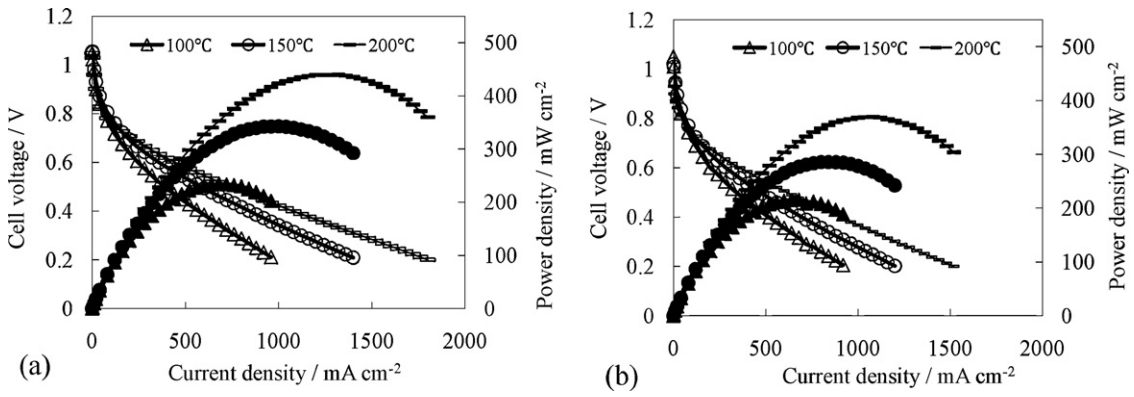

Fig. 9. Performance of H_2/O_2 fuel cells with (a) the H_3PO_4-doped PBI/SAPO composite membrane and (b) the H_3PO_4-doped PBI membrane.

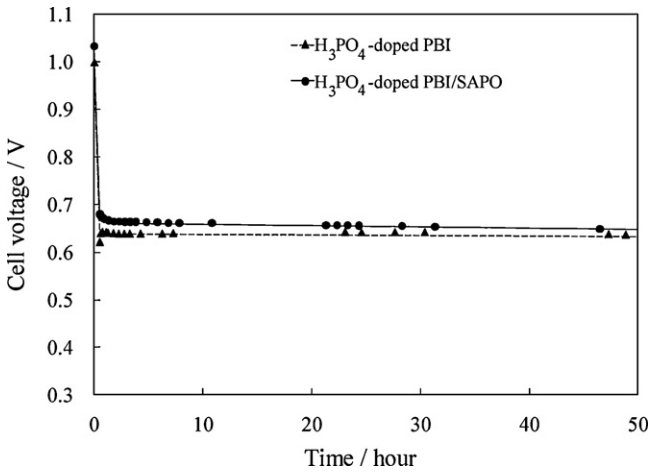

Fig. 10. Changes in the cell voltages of H_2/O_2 fuel cells with the H_3PO_4-doped PBI/SAPO composite membrane and the H_3PO_4-doped PBI membrane at 150 °C. The current density was maintained at a constant value of 200 mA cm^{-2}.

of 2–3 mV $decade^{-1}$, as can be seen in Fig. 10. EIS measurements showed that the decrease in cell voltage was mainly attributable to an increase in the polarization resistance rather than the ohmic resistance. For example, the polarization resistance of the fuel cell with the composite membrane increased from 1.1 to 1.5 Ω cm^2. Because the dissolution of Pt in acid solutions is considerable when the cathode potential is over 800 mV [27], it appears that the deterioration observed above is not mainly due to agglomeration of the Pt particles in the Pt/C cathode during cell discharge. An alternative explanation is that a part of the amorphous carbon in the catalyst support is transformed into graphitic carbon, resulting in a significant decrease in the surface area of carbon [28]. If this second explanation is correct, then one could avoid such deterioration by using a graphite-rich catalyst support. In any event, we emphasize that the composite membrane retained a constant ohmic value of 0.16 Ω cm^2 for at least 50 h.

4. Conclusions

A PBI-based composite membrane was successfully developed using SAPO particles as inorganic fillers. The SAPO particles were synthesized by the reaction of SnO_2 and $Al(OH)_3$-mixed powders with an H_3PO_4 solution in the PBI membrane at a temperature of 250 °C. This composite membrane was thermally stable in air until at least 500 °C. Homogenous dispersion of the SAPO particles was obtained in the composite membrane, wherein networks of proton pathways were interrupted at places. The upper limit of the H_3PO_4-doping level for the PBI/SAPO composite membrane was determined to be 114 wt%. Two types of protons were found in the H_3PO_4-doped PBI/SAPO composite membrane: protons in the H_3PO_4 molecules and protons incorporated into the SAPO particles. Interaction between these protons provided proton conductivities several times higher than those of the H_3PO_4-doped PBI membrane in the temperature range from 50 to 300 °C. As a result, the present composite membrane yielded a better cell performance at high temperatures compared to the H_3PO_4-doped PBI membrane. Furthermore, a high durability of the composite membrane was also confirmed during cell discharge.

References

[1] Q. Li, R. He, J.O. Jensen, N.J. Bjerrum, Chem. Mater. 15 (2003) 4896–4915.
[2] O. Savadogo, J. Power Sources 127 (2004) 135–161.
[3] J. Zhang, Z. Xie, J. Zhang, Y. Tang, C. Song, T. Navessin, Z. Shi, D. Song, H. Wang, D.P. Wilkinson, Z. Liu, S. Holdcroft, J. Power Sources 160 (2006) 872–891.
[4] Y. Shao, G. Yin, Z. Wang, Y. Gao, J. Power Sources 167 (2007) 235–242.
[5] J. Mader, L. Xiao, T.J. Schmidt, B.C. Benicewicz, Adv. Polym. Sci. 216 (2008) 63–124.
[6] Q. Li, J.O. Jensen, R.F. Savinell, N.J. Bjerrum, Prog. Polym. Sci. 34 (2009) 449–477.
[7] J.A. Asensio, E.M. Sanchez, P. Gomez-Romero, Chem. Soc. Rev. 39 (2010) 3210–3239.
[8] M. Kawahara, J. Morita, M. Rikukawa, K. Sanui, N. Ogata, Electrochim. Acta 45 (2000) 1395–1398.
[9] M. Litt, R. Ameri, Y. Wang, R. Savinell, J. Wainwright, Mater. Res. Soc. Symp. Proc. 548 (1999) 313–323.
[10] R. He, Q. Li, G. Xiao, N.J. Bjerrum, J. Membr. Sci. 226 (2003) 169–184.
[11] P. Staiti, M. Minutoli, S. Hocevar, J. Power Sources 90 (2000) 231–235.
[12] P. Staiti, M. Minutoli, J. Power Sources 94 (2001) 9–13.
[13] P. Staiti, Mater. Lett. 47 (2001) 241–246.
[14] S. Oh, T. Yoshida, G. Kawamura, H. Muto, M. Sakai, A. Matsuda, J. Mater. Chem. 20 (2010) 6359–6366.
[15] M. Li, Z. Shao, K. Scott, J. Power Sources 183 (2008) 69–75.
[16] Y. Yamazaki, M. Jang, T. Taniyama, Sci. Technol. Adv. Mater. 5 (2004) 455–459.
[17] M. Jang, Y. Yamazaki, J. Power Sources 139 (2005) 2–8.
[18] A. Tomita, N. Kajiyama, T. Kamiya, M. Nagao, T. Hibino, J. Electrochem. Soc. 154 (2007) B1265–B1269.
[19] Y.C. Jin, S.B. Shen, T. Hibino, J. Mater. Chem. 20 (2010) 6214–6217.
[20] K.D. Kreuer, Chem. Mater. 8 (1996) 610–641.
[21] L. Xiao, H. Zhang, E. Scanlon, L.S. Ramanathan, E.W. Choe, D. Rogers, Chem. Mater. 17 (2005) 5328–5333.
[22] R.F. Savinell, M.H. Litt, US Patent, 5,716,727 (1998).
[23] P. Heo, N. Kajiyama, K. Kobayashi, M. Nagao, M. Sano, T. Hibino, Electrochem. Solid-State Lett. 11 (2008) B91–B95.
[24] M. Nagao, T. Kamiya, P. Heo, A. Tomita, T. Hibino, M. Sano, J. Electrochem. Soc. 153 (2006) A1604–A1609.
[25] S.R. Samms, S. Wasmus, R.F. Savinell, J. Electrochem. Soc. 143 (1996) 1225–1232.
[26] H. Matsumoto, Y. Furuya, S. Okada, T. Tanji, T. Ishihara, Sci. Technol. Adv. Mater. 8 (2007) 531–535.
[27] A. Honji, T. Mori, K. Tamura, Y. Hishinuma, J. Electrochem. Soc. 135 (1988) 355–359.
[28] G.A. Gruver, J. Electrochem. Soc. 125 (1978) 1719–1720.